A Human Ferritin Iron Oxide Nano-composite Magnetic Resonance Contrast Agent

Masaki Uchida,[1,2] Masahiro Terashima,[3] Charles H. Cunningham,[4] Yoriyasu Suzuki,[3] Deborah A. Willits,[1,5] Ann F. Willis,[1,2] Philip C. Yang,[3] Philip S. Tsao,[3] Michael V. McConnell,[3] Mark J. Young,[2,5] and Trevor Douglas[1,2*]

Macrophages play important roles in the immunological defense system, but at the same time they are involved in inflammatory diseases such as atherosclerosis. Therefore, imaging macrophages is critical to assessing the status of these diseases. Toward this goal, a recombinant human H chain ferritin (rHFn)-iron oxide nano composite has been investigated as an MRI contrast agent for labeling macrophages. Iron oxide nanoparticles in the form of magnetite (or maghemite) with narrow size distribution were synthesized in the interior cavity of rHFn. The composite material exhibited the R_2 relaxivity comparable to known iron oxide MRI contrast agents. Furthermore, the mineralized protein cages are readily taken up by macrophages in vitro and provide significant T2* signal loss of the labeled cells. These results encourage further investigation into the development of the rHFn-iron oxide contrast agent to assess inflammatory disease status such as macrophage-rich atherosclerotic plaques in vivo. Magn Reson Med 60:1073–1081, 2008.

Key words: ferritin; MR contrast agent; macrophage; inflammation; atherosclerosis

Macrophages are considered an important component of the immunological defense system (1). They provide both innate and acquired immunity and protect the host from invading pathogens. Conversely, due to their function in the development of inflammatory response, macrophages are associated with inflammatory diseases such as tuberculosis (2), legionellosis (3), rheumatoid arthritis (4,5), cirrhosis (6), and atherosclerosis (1,7). Imaging macrophages in these lesions may allow us to assess the status of inflammation and disease.

Among diseases in which macrophages are involved, atherosclerosis caused by plaques is one of the most important targets for medical diagnosis and treatment because coronary artery disease is one of the major causes of death in western countries. Accumulating evidence indicates that macrophages take part in the initiation of plaques to the state that ultimately leads to rupture (7,8). Consequently, macrophages are an appropriate target to evaluate the inflammatory status of plaques (9,10). Recent advances in magnetic resonance imaging (MRI) technology has allowed for the noninvasive visualization of atherosclerotic plaques. For example, ultrasmall superparamagnetic iron oxide (USPIO) contrast agents, such as ferumoxtran-10 (Combidex®), have been evaluated as potential MRI contrast agents to detect macrophages within plaques (8–13). Not only in vitro but also in vivo studies warrant potentiality of USPIOs to evaluate the plaque condition, because it has been confirmed that USPIOs which administrated systemically in vivo accumulate in macrophage in atherosclerotic plaque of rabbits and human (8,11). However, their uptake efficiency into macrophage may be suboptimal (9,10).

We have recently shown that protein cage architectures, such as virus capsids (14,15), ferritins (15,16), and heat shock proteins (17), are useful templates for the synthesis of ferrimagnetic nanomaterials encapsulated within the interior cavity of the protein cage. These nano materials are comparable in size to USPIO contrast agents but possess unique features not present in the commercially available USPIO contrast agents. This includes the fact that protein cage architectures are precise assemblies of subunits with an extremely homogeneous size distribution (18). The homogeneity of the protein cage template leads to homogeneity of the templated iron oxide nanoparticles within the protein cage architecture. Furthermore, protein cage templates possess three distinct interfaces, that is, interior surface of the cage, exterior surface of the cage, and the interface between subunits, which can be chemically and/or genetically modified to impart novel function by design to the template including targeting and therapeutic delivery (18). In addition, these highly symmetrical protein cage architectures provide an ideal multivalent platform for attachment and presentation of Gd(III) binding chelates to generate materials with very high R_1 relaxivity (19–23). These features suggest that protein cage nanoparticle composites have the potential to serve as a new class of T_1 and T_2 MRI contrast agents.

The aim of this study was to characterize the MRI properties of a ferritin protein cage-iron oxide nano-composite material and investigate its use as an USPIO MRI contrast agent to label macrophages.

[1]Department of Chemistry and Biochemistry, Montana State University, Bozeman, Montana.
[2]Center for Bio-Inspired Nanomaterials (CBIN), Montana State University, Bozeman, Montana.
[3]Division of Cardiovascular Medicine, Stanford University School of Medicine, Stanford, California.
[4]Department of Medical Biophysics, Sunnybrook Health Sciences Centre, Toronto, Ontario, Canada.
[5]Department of Plant Sciences, Montana State University, Bozeman, Montana.
Grant sponsor: the National Institutes of Health; Grant number: R21EB005364; R01HL078678.
Disclosure: M. McConnell receives research support from GE Healthcare and is on the Scientific Advisory for Kowa Pharmaceuticals. M. Young and T. Douglas hold shares in Specigen, Inc.
*Correspondence to: Trevor Douglas, Montana State University, Department of Chemistry and Biochemistry, 113 Chemistry and Biochemistry Building, Bozeman, MT 59715. E-mail: tdouglas@chemistry.montana.edu
Received 8 January 2008; revised 8 May 2008; accepted 20 June 2008.
DOI 10.1002/mrm.21761
Published online in Wiley InterScience (www.interscience.wiley.com).

MATERIALS AND METHODS

Cloning and Purification of Recombinant Human H Chain Ferritin (rHFn)

The cloning, heterologous expression, and purification of recombinant human H chain ferritin (rHFn) has been described previously (16). Briefly, the gene encoding the HFn was amplified by polymerase chain reaction (PCR) followed by cloning into the *Nde*I/*Bam*HI restriction endonuclease sites of the pET-30a(+) (Novagen, Madison, WI) for expression of the full-length HFn protein. The HFn clone was expressed in and purified from *E. coli* (BL21 (DE3): Novagen). Cells were harvested by centrifugation and subsequently resuspended in 45 mL of lysis buffer (100 mM HEPES, pH 8.0, 50 mM NaCl, 50 μg/mL of Lysozyme, 60 μg/mL of DNAse, 100 μg/mL of RNAse). The suspension was incubated for 30 min at room temperature followed by cell disruption by a combination of French Press lysis and sonication on ice. The solution was centrifuged to remove cell debris and the resulting supernatant heated at 60°C for 10 min to precipitate many of the *E. coli* proteins, which were subsequently removed by centrifugation. The resulting supernatant was subjected to size exclusion chromatography (SEC: Amersham-Pharmacia, Piscataway, NJ) using a Superose 6 column to isolate intact assembled rHFn protein cages. The purified rHFn protein cages were further characterized by UV/Vis spectroscopy, dynamic light scattering (DLS: Brookhaven, 90Plus particle size analyzer) and transmission electron microscopy (TEM: LEO 912AB).

Iron Oxide Mineralization and Characterization

Iron oxide mineralization constrained within the rHFn protein cage structure was performed under three different iron loading factor conditions, that is, 1000Fe, 3000Fe, and 5000Fe per cage, respectively. Briefly, 10 mL solution of the rHFn (10 mg, 19.8 nmol in 100 mM NaCl) was added to a jacketed reaction vessel under a N_2 atmosphere. The temperature of the vessel was brought up to and maintained at 65°C by circulating water through the jacketed flask. The pH was titrated to 8.5 with 50 mM NaOH (718 Auto Titrator, Brinkmann). Ammonium iron(II) sulfate hexahydrate ($(NH_4)_2Fe(SO_4) \cdot 6H_2O$) and hydrogen peroxide (H_2O_2) were used as an iron source and oxidant, respectively. To achieve a theoretical Fe loading factor of 1000Fe, 3000Fe, and 5000Fe per protein cage, 1580, 4741, and 7901 μL of $(NH_4)_2Fe(SO_4) \cdot 6H_2O$ solution (12.5 mM) were used in independent reactions, respectively. Because the mineralization reaction proceeds according to reaction 1, stoichiometric equivalents of freshly prepared degassed H_2O_2 (4.17 mM) was also added as an oxidant. The $(NH_4)_2Fe(SO_4) \cdot 6H_2O$ and H_2O_2 solutions were injected simultaneously into the reaction vessel at a constant rate of 158 μL/min (100Fe/(cage · min)) using a syringe pump (Kd Scientific). After the mineralization procedure, 200 μL of 300 mM sodium citrate was added to chelate any remaining free Fe, and the sample was dialyzed against Dulbecco's Phosphate Buffered Saline (DPBS). The mineralized rHFn was purified from any aggregation products and analyzed by SEC with Superose 6 while monitoring absorbance at 280 nm and 410 nm for elution of protein and mineral, respectively. Only mono-dispersed mineralized rHFn was used for subsequent experiments.

$$3Fe^{2+} + H_2O_2 + 2H_2O \xrightarrow{65^\circ C} Fe_3O_4 + 6H^+ \quad [1]$$

MR Relaxivity Measurements and MR Imaging of the Mineralized rHFn

Each sample was serially diluted from 8 mM to 0.1 mM (Fe concentration) in DPBS. One hundred microliters of each solution was added in a 96-well PCR plate (E&K Scientific Products, Inc., Santa Clara, CA) and embedded in 1% agarose supplemented with 1% $CuSO_4$ (24). Measurements were performed using a 1.5 Tesla (T) whole-body scanner (GE Healthcare, Waukesha, WI) equipped with a 5-inch receive-only surface coil. To measure longitudinal relaxation times (T_1), an inversion recovery spin echo (IR-SE) sequence was used (T_R = 6000 ms T_E = 9 ms, T_I = 50, 100, 150, 200, 250, 300, 350, 400, 450, 550, 650, 750, 850, 950, 2000, and 3000 ms, matrix = 128 × 128, slice thickness = 3.0 mm, NEX = 1, field of view [FOV] = 12 cm). For the measurement of transverse relaxation times (T_2), a spin-echo sequence with different echo times was used (T_R = 3000 ms T_E = 9, 12, 20, 30, 50, 80, 100, and 160 ms, matrix = 192 × 160, slice thickness = 3.0 mm, NEX = 1, FOV = 12 cm). The T_1 for each sample was calculated in MATLAB (The Mathworks, Natick, MA) by using the fminsearch routine to perform a nonlinear fit of the data to the inversion-recovery signal equation. The T_2 for each sample was also calculated using fminsearch, but by fitting to a mono-exponential decay curve. Relaxivity, R_1 and R_2, of each sample were calculated using the T_1 and T_2 data and Fe concentration determined by an inductively coupled plasma mass spectrometry (ICP-MS: Agilent, Santa Clara, CA). To assess the relative visual signal at 1.5T, the images were acquired by using a gradient echo (GRE) sequence (T_R = 100 ms T_E = 10 ms, Flip angle = 30°, matrix = 256 × 256, slice thickness = 3.0 mm, NEX = 1, FOV = 12 cm).

In Vitro Contrast Agent Uptake Assay

Murine macrophage cells (RAW) were cultured using Dulbecco's Modified Eagle Medium (DMEM, cat. 11995-065, Invitrogen, Carlsbad, CA) supplemented with 10% fetal bovine serum, 100 units/mL of penicillin, 100 μg/mL of streptomycin at 37°C in 5% CO_2 atmosphere. Cells were passaged every 2–3 days.

Uptake of the mineralized rHFn with various Fe loading factors was evaluated using ICP-MS and Prussian blue staining under two different conditions, that is, constant rHFn concentration and constant Fe concentration. In the case of the constant rHFn condition, the mineralized rHFn was added to a final concentration of 0.3 mg/mL (equivalent to 33 μg Fe/mL, 100 μg Fe/mL and 165 μg Fe/mL for 1000Fe, 3000Fe, and 5000Fe per rHFn cage, respectively). In the case of constant Fe concentration, the mineralized rHFn was added to a final concentration of 165 μg Fe/mL (equivalent to 1.5 mg rHFn/mL, 0.5 mg rHFn/mL, and 0.3 mg rHFn/ mL for 1000Fe, 3000Fe, and 5000Fe per HFn cage, respectively). For comparison, cells were also incu-

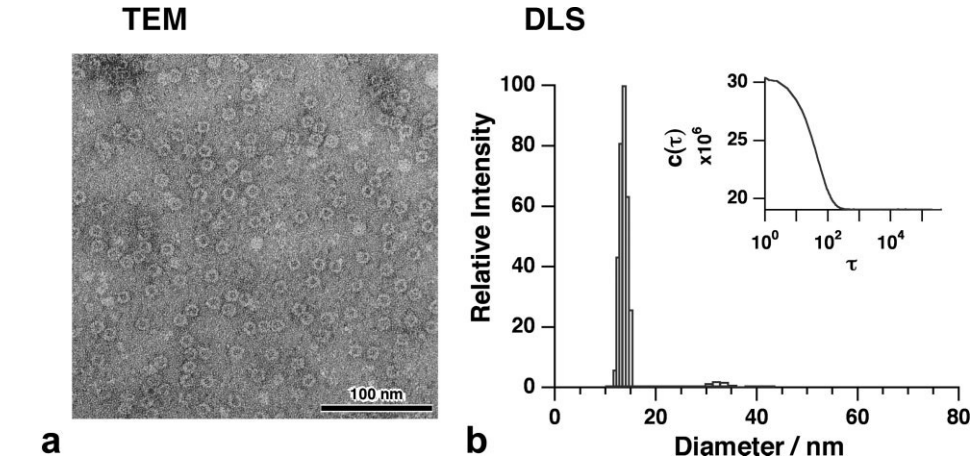

FIG. 1. **a:** TEM micrograph of the purified rHFn negatively stained with uranyl acetate. The rHFn cages have homogeneous size distribution. **b:** DLS analysis of the purified rHFn showed mode diameter of 13.2 nm and mean diameter of 13.5 nm. (The inset is corresponding correlation function.)

bated with 165 μg Fe/mL of Fe based MR contrast agent, ferumoxides or ferumoxtran-10 (i.e., Feridex® and Combidex®, respectively, AMAG Pharmaceuticals, Inc., Cambridge, MA).

For the analysis using ICP-MS, cells were seeded into six-well polystyrene plate at the concentration of 1×10^6 cells/ well. After 24 h of incubation, the medium was removed and 1.6 mL of a solution containing a mixture of the fresh cell culture medium and the mineralized rHFn samples at a ratio of 3:1 was added to a well. The cells were further incubated with the mineralized rHFn at 37°C in 5% CO_2 atmosphere for 24 or 72 h. After incubation, the solution was aspirated and the cells gently washed two times with DPBS followed by adherent cell removal and collection using 0.25% trypsin-EDTA (25200-056, Invitrogen). The number of viable cells was determined by trypan blue exclusion assay and counting using a hemocytometer. To quantify the amount of Fe taken up by the cells, cell pellets were dissolved in nitric acid and subjected to ICP-MS analysis. The data were assessed using a Student's t-test.

For analysis of Fe uptake by Prussian blue staining, cells were cultured in a four-well slide glass chamber in the same manner as described above. Subsequently, the cells were fixed with 4% of formaldehyde then washed with distilled water three times. Five percent of potassium ferrocyanide was mixed with 5% hydrochloric acid at a ratio of 1:1 just before use for staining. Fixed cells were incubated with the mixed solution for 30 min at room temperature, washed by distilled water three times, and counterstained with Nuclear Fast Red.

MRI of Macrophage Cells

Macrophages were incubated with 165 μg Fe/mL of the mineralized rHFn, ferumoxides or Ferumoxtran-10 for 24 h in the same manner as described above for the uptake assay. Then, 1×10^6 cells were suspended in 100 μL of DPBS, transferred in a 96-well PCR plate and allowed to settle by gravity. The MR imaging of the cells was performed at 1.5T with the same setup described above using a GRE sequence (T_R = 100 ms T_E = 10 ms, Flip angle = 30°, matrix = 256 × 256, slice thickness = 1.0 mm, NEX = 1, FOV = 12 cm).

RESULTS

Characterization of Mineralized rHFn

Recombinant human H chain ferritin (rHFn) was used as an active, constrained reaction template for the synthesis of ferrimagnetic iron oxide nanoparticles for application as an MRI contrast agent. Analysis by TEM demonstrated that rHFn has a cage-like architecture of approximately 12-nm diameter, which is identical to native mammalian ferritins (Fig. 1) (25). Dynamic light scattering analysis also demonstrated that the rHFn protein cage is monodispersed (mean size = 13.5 nm), suggesting that the heterologously expressed rHFn is assembled from 24 identical subunits to form a spherical architecture with 4:3:2 symmetry.

The spatially selective synthesis of an iron oxide nanoparticle within the rHFn protein cage architecture is supported by multiple lines of evidence. In the presence of the purified rHFn, a dark brown solution formed with no visible precipitation, whereas in protein-free control reactions there was an immediate formation of a bulk precipitate. TEM analysis of nonstained rHFn samples, after the iron oxide synthesis reactions, revealed electron dense nanoparticles with narrow size distributions (Fig. 2). The average size of the particles increased from 3.6 to 5.9 nm with increasing Fe loading factor from 1000Fe to 5000Fe per cage. Indexing of selected area electron diffraction patterns revealed that these particles were crystalline material. The measured d-spacing of the particles was compared with the Joint Committee on Powder Diffraction Standards (JCPDS) and confirmed to be ascribed to either maghemite (γ-Fe_2O_3) or magnetite (Fe_3O_4) (Fig. 3). Due to the similarity in lattice constants for these two cubic structures (a= 8.352 of maghemite or a= 8.396 of magnetite, both from JCPDS), it is difficult to unambiguously distinguish them from the electron diffraction patterns alone. Further structural characterization of the mineralized rHFn is not significant in this study because the magnetic properties of maghemite and magnetite are similar due to their similarity of crystal structure. The theoretical core diameters calculated for a uniform spherical particle of the cubic iron oxide (either Fe_3O_4 or γ-Fe_2O_3) phase at loading factor of 1000Fe, 3000Fe, and 5000Fe are 3.6 nm, 5.2 nm, and 6.2 nm, respectively. The observed mean diameter of the iron oxide core formed inside of the HFn are close to

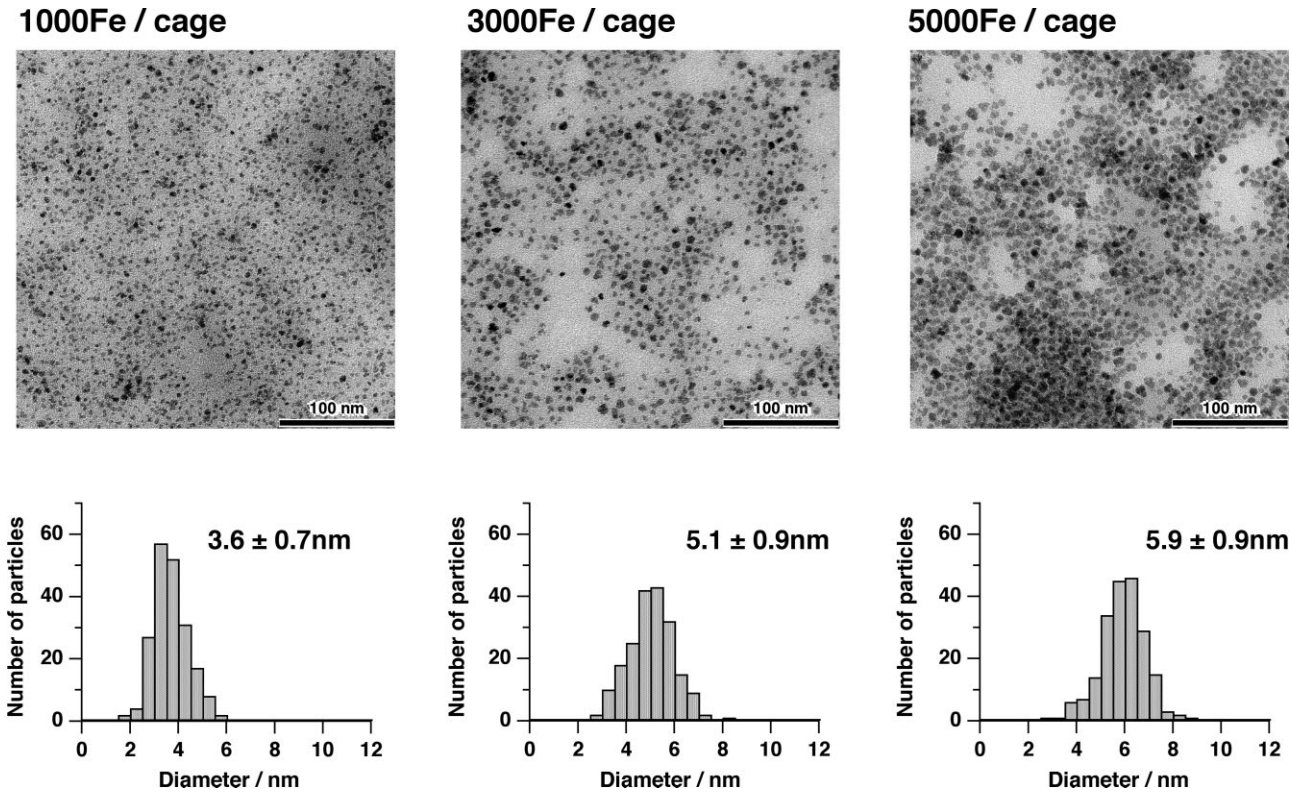

FIG. 2. TEM micrographs of mineralized particles within rHFn with various Fe loading factors (top). Size distribution histograms of the particles analyzed from the TEM images (bottom). The value shown on the histograms are mean ± standard deviation. The size of the particles increase with increasing Fe loading factor per cage.

the theoretical value (Fig. 2). This suggests that almost all Fe added during the reaction are accumulated inside of the HFn cage. This is favorable character of HFn for template iron oxide core formation. Because interior cavity of HFn in which iron oxide is formed is approximately 8 nm in diameter (25), it is large enough to accumulate Fe as an iron oxide even at the loading factor of 5000Fe/cage. SEC analysis of the mineralized rHFn demonstrated the co-elution of the protein cage and the iron oxide indicating the composite nature of rHFn - iron oxide nanoparticle (Fig. 4a). Furthermore, both the pre- and postmineralized rHFn had identical SEC retention times, indicating that the overall size of the protein cage had not been altered by the iron oxide synthesis reaction (Fig. 4a).

However, a smaller peak on the leading edge of the SEC profile after the mineralization is probably due to aggregated rHFn during the mineralization process but was easily separated by chromatography. DLS analysis of the mineralized rHFn after SEC purification indicates that the protein cage is approximately 14 nm in diameter, which is nearly identical to intact rHFn before mineralization (Figs. 1b, 4b). In combination, these results demonstrate that the synthesis of magnetite (or maghemite) nanoparticles occurred specifically within the interior cavity of the rHFn protein cage without significantly perturbing the overall protein cage architecture.

MR Relaxivity Measurement and Imaging of the Mineralized rHFn

To evaluate the potential of the iron oxide mineralized rHFn as an MRI contrast agent, MR relaxivity determination and imaging of the synthesized materials was performed (Fig. 5). As shown in Figure 5, the T_2* signal loss

a

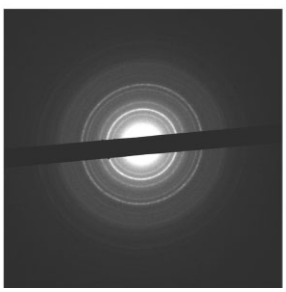

b

Measured d-spacing	d-spacing of maghemite	d-spacing of magnetite
3.00	2.953	2.967
2.54	2.518	2.532
2.08	2.089	2.099
1.64	1.607	1.616
1.49	1.476	1.485

FIG. 3. **a:** Selected area electron diffraction of the mineralized rHFn with loading factor of 3000Fe per cage. **b:** Measured d-spacing of the mineralized rHFn (300Fe/cage) and the reported d-spacing for maghemite (JCPDS #39-1346) and magnetite (JCPDS #19-0629). The mineralized particles show powder diffraction patterns corresponding to either maghemite (γ-Fe_2O_3) or magnetite (Fe_3O_4).

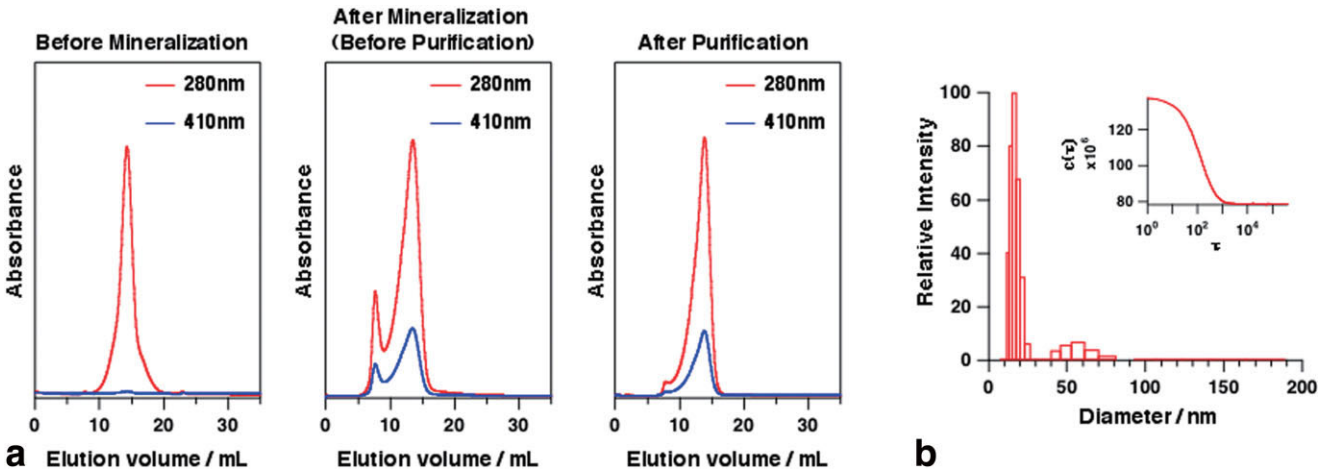

FIG. 4. **a:** SEC of rHFn before mineralization reaction, after mineralization reaction with 3000Fe/cage (before purification) and after purification. **b:** DLS analysis of the mineralized rHFn after purification. Co-elution profile of rHFn (280 nm) and iron oxide (410 nm) in the SEC after mineralization reaction indicate the composite nature of the mineralize rHFn. SEC and DLS of the mineralized HFn after purification indicate that the protein cages are almost mono dispersed.

became larger with increasing Fe loading factor per cage under the same Fe concentration. The image of HFn5000Fe was similar to that of ferumoxides and ferumoxtran-10. Likewise, R_1 and R_2 relaxivities of the mineralized rHFn increased with increasing Fe loading factor. The R_1 and R_2 of HFn5000Fe were comparable to that of ferumoxides and ferumoxtran-10. These results indicate that mineralized rHFn protein cages could have similar T_1/T_2* MR imaging properties to known iron-oxide contrast agents. Previous measurements on magneto-ferritin having iron oxide cores of 7.3 ± 1.4 nm diameter reported higher values of R_2 (26) due to the larger particle size as compared with this study (3.6 ± 0.7 nm, 5.1 ± 0.9 nm and 5.9 ± 0.9 nm). This strongly supports the concept that these ferritin cages act as reaction vessels with significant control over particle size and associated magnetic properties.

Uptake Assay and MR Imaging of Macrophage Cells

The mineralized rHFn cages were taken up by the macrophages regardless of Fe loading factor per cage. As the Prussian blue staining results show, mineralized rHFn cages were phagocytosed by the RAW cells to a similar degree as ferumoxides (Fig. 6) when the same Fe amount was added. On the other hand, only limited staining was observed in the cells incubated with ferumoxtran-10, even though the cells were treated with the same amount of Fe as the cells treated with other contrast agents.

Quantitative analysis of Fe uptake determined by ICP-MS (Fig. 7) showed results similar to the Prussian blue staining. Cells incubated at constant rHFn concentration, with 1000Fe, 3000Fe, and 5000Fe per cage accumulated 18 pg/cell, 52 pg/cell, and 116 pg/cell of Fe after 72 h of incubation, respectively. This suggests that the RAW cells phagocytosed nearly identical amounts of rHFn protein cages, irrespective of Fe loading factor per cage. Even when the RAW cells were incubated at fixed Fe concentration, the cells took up more Fe with increasing Fe loading factor in the cage they treated with (21 pg/cell, 71 pg/cell, and 116 pg/cell after 72 h of incubation, respectively). These results suggest that loading more Fe per cage is advantageous not only from large T2* signal loss but also effective Fe uptake by macrophage. At equivalent Fe concentration, the amount of Fe taken up by the cells cultured with the mineralized protein cage was less than that of cells cultured with ferumoxides. Ferumoxide incubation resulted in 152 pg Fe/cell after 72 h, and statistical comparison with Fe uptake from ferritin incubation

	rHFn1000Fe	rHFn3000Fe	rHFn5000Fe	Ferumoxides	Ferumoxtran-10
R1 / $(mM \cdot s)^{-1}$	2.3	4.2	8.4	7.8	12
R2 / $(mM \cdot s)^{-1}$	11	31	93	119	101
GRE image					

FIG. 5. R_1 and R_2 relaxivity and GRE images of the mineralized rHFn, ferumoxides and ferumoxtran-10 at 1.5T. Each sample was in DPBS in a 96-well micro titer plate and embedded in an agarose gel.

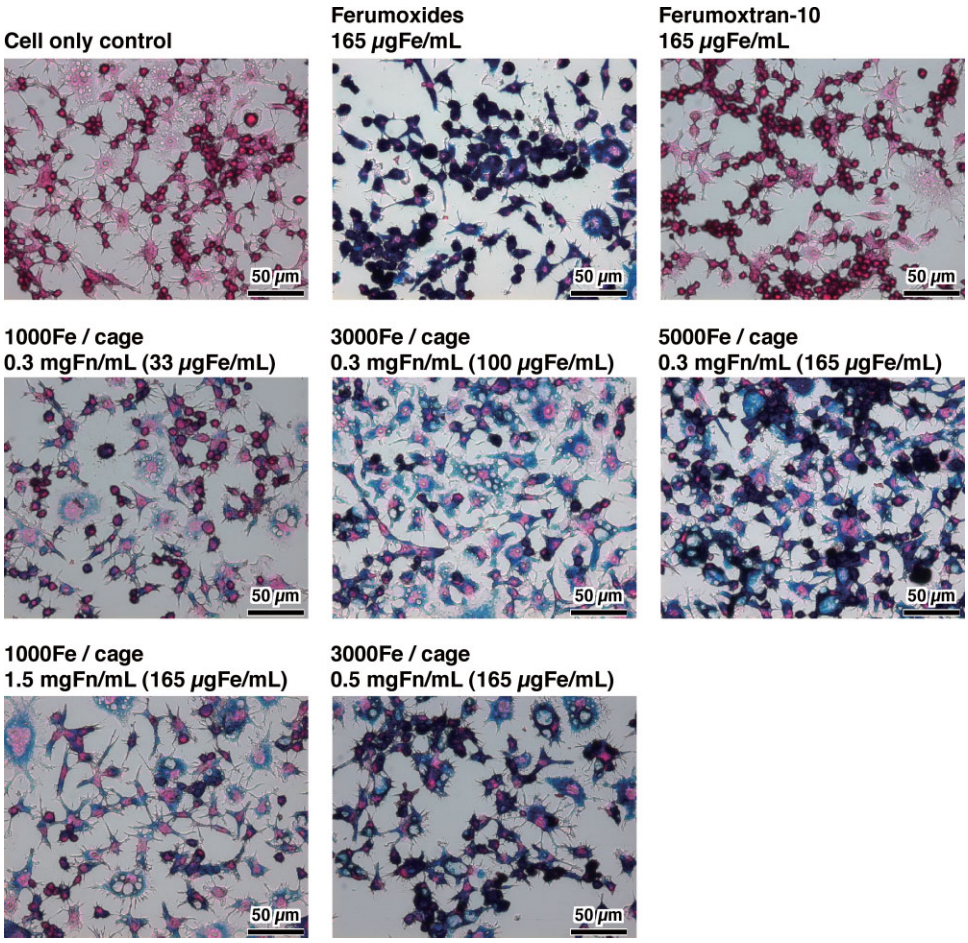

FIG. 6. Optical micrographs of Prussian blue staining of RAW macrophages incubated for 24 h with mineralized rHFn under various loading factors of Fe per cage.

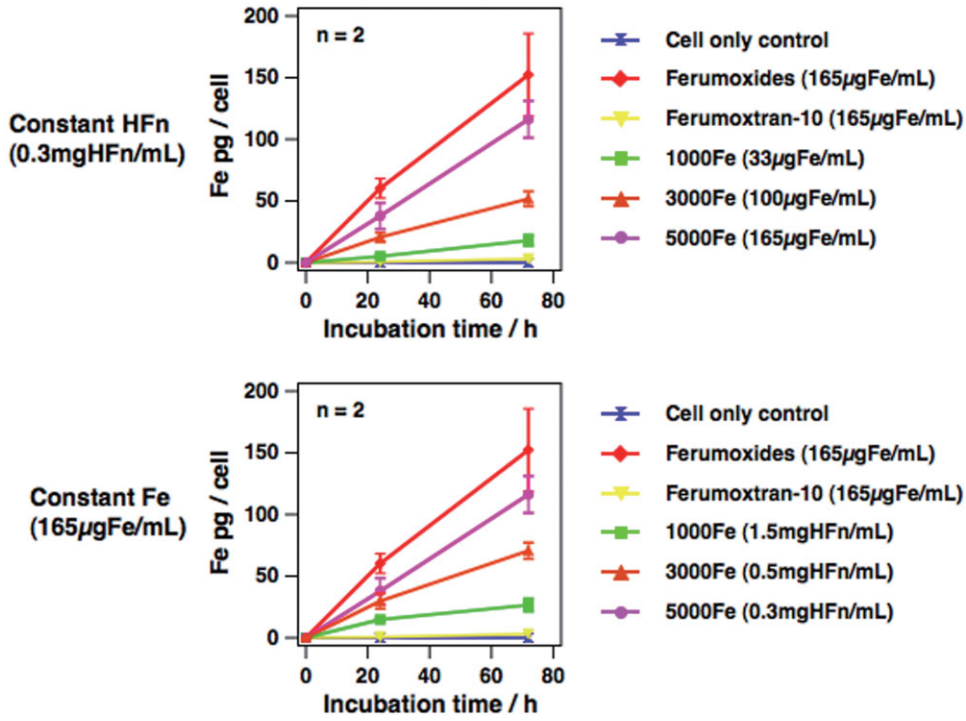

FIG. 7. Fe content in RAW macrophages incubated with mineralized rHFn, Ferumoxides or Ferumoxtran-10 for up to 72 h under two different conditions, that is, a constant rHFn concentration of 0.3 mgHFn/cage (upper) and a constant Fe concentration 165 μgFe/mL (lower). Fe concentration was analyzed using ICP-MS. Amount of Fe taken up by macrophages cultured with HFn5000Fe was comparable with that cultured with Ferumoxides ($P = 0.3$). All the mineralized rHFn are taken up statistically more than Ferumoxtran-10 under both conditions ($P < 0.05$).

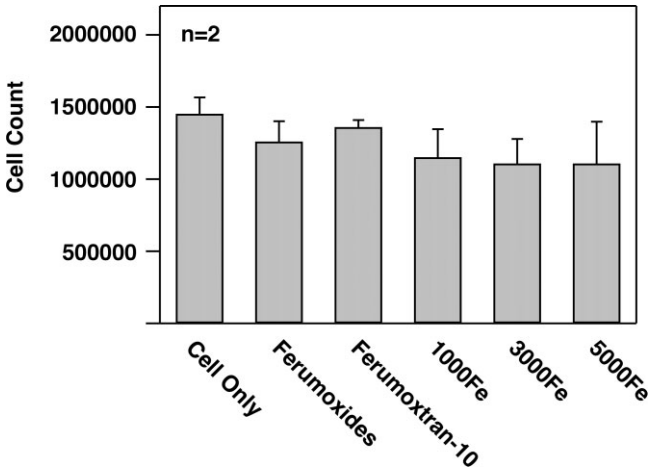

FIG. 8. Trypan blue dye cell viability assay of macrophage incubated with mineralized rHFn at 0.3 mgHFn/mL for 24 h.

yielded $P = 0.03$, 0.08, and 0.3 for HFn1000Fe, 3000Fe, and 5000Fe, respectively. However, significantly more Fe was accumulated in cells incubated with rHFn than cells cultured with ferumoxtran-10. Ferumoxtran-10 incubation resulted in 3 pg Fe/cell after 72 h, and statistical comparison with Fe uptake from ferritin incubation yielded $P = 0.02$, 0.005, and 0.009 for HFn1000Fe, 3000Fe, and 5000Fe, respectively. Cell viability data for cells only vs. cells incubated with the various contrast agents (Fig. 8) did show some decrease in cell count for the contrast agents but this was not statistically significant ($P > 0.05$).

Labeled macrophages showed a wide range of T_2* signal loss by MRI whereas cells without any contrast had no signal loss under the same total Fe concentration (Fig. 9). The signal loss from incubated cells became larger across the agents ferumoxtran-10, rHFn 1000Fe/cage, 3000Fe/cage, 5000Fe/cage, and ferumoxides. It should be noted that although the R_2 relaxivities of rHFn 1000Fe/cage, and rHFn 3000Fe/cage were less than that of ferumoxtran-10, the MRI signal loss of cells labeled with the mineralized rHFn was greater than that of the cells labeled with ferumoxtran-10. This is likely due to greater uptake of rHFn protein cages by macrophages in vitro than ferumoxtran-10.

DISCUSSION

We have demonstrated the potential of using a biomimetic approach for developing a new class of MRI contrast agents using a protein cage, human ferritin, to image macrophages in vitro as the first step to the assessment of inflammatory diseases, such as atherosclerosis. The natural role of ferritin is the sequestration of Fe as a hydrated ferric oxide (25,27), and it is, therefore, an appropriate reaction vessel for ferrimagnetic iron oxide synthesis. In the present study, rHFn was exploited as a template for superparamagnetic iron oxide nanoparticle synthesis for use as an MRI contrast agent. The protein cage mediated iron oxide nanoparticles were compared with iron oxide MR contrast agents, such as dextran-coated ferumoxides and ferumoxtran-10, to evaluate cell uptake and the MR signal properties.

The important findings of this study are that the mineralized protein cages are readily taken up by macrophages in vitro and provide strong T_2* MR contrast. This suggests that this material has a great potential as an MRI contrast agent to assess inflammatory status such as atherosclerotic plaque progression/regression. At equivalent iron concentrations, ferumoxides are taken up by the macrophages more than the mineralized rHFn using an in vitro cellular uptake assay (Figs. 6, 7). However, likely due to their larger size, ferumoxides are trapped by Kupffer cells in liver tissue during first-pass after injection (28,29), reducing their circulation time, making them less useful for macrophage and atherosclerosis imaging in vivo. On the other hand, ferumoxtran-10 can reach atherosclerotic lesions in vivo (8,11), likely due to a longer circulation time. These materials have been examined as potential contrast agents to image macrophage-rich plaques. However, their uptake efficiency into macrophage may be suboptimal. The overall size of the mineralized rHFn protein cages (14 nm, Fig. 1b) is closer to that of ferumoxtran-10 (29.5 $\pm$ 23.1 nm) (30) rather than that of ferumoxides (58.5 $\pm$ 185.8 nm) (30). Nevertheless, cells incubated with the rHFn protein cages took up statistically significantly more ($P < 0.05$) iron than those incubated with ferumoxtran-10 (7- to 39-fold more) at the same Fe incubation concentration, and cell uptake levels were fairly comparable to the ferumoxides. This indicates that the protein cage based contrast agents have significant potential for labeling macrophages within inflammatory lesion such as atherosclerotic plaques, warranting in vivo evaluation. The incorporation of iron oxide nanoparticle within rHFn can be controlled precisely with a very narrow size distribution (Fig. 2). Because the size of a magnetic particle is a significant factor, with a large effect on the MRI properties, precise control of the iron oxide particle size may be advantageous.

Another significant advantage of the cage-based material may be that the protein cage can serve not only as a template for iron oxide nanoparticle synthesis but also as a platform for imparting additional functionality such as cell-specific targeting capability (16,31,32). Protein cages such as ferritin are self-assembled from a limited number of protein subunits into precisely defined architectures. The exterior and interior surfaces of a cage possess chem-

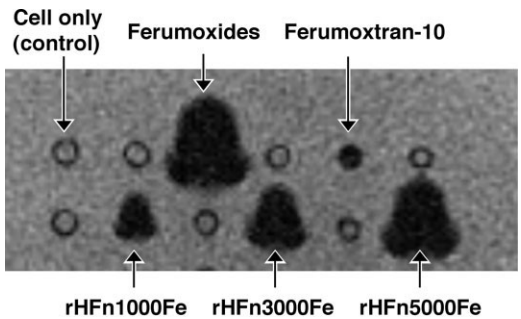

FIG. 9. In vitro MR images of RAW macrophage cells incubated with 165 μg Fe/mL of mineralized rHFn, ferumoxides or ferumoxtran-10 for 24 h. The cells were suspended in DPBS and allowed to settle by gravity. The MR imaging was performed at 1.5T.

ically addressable functional groups. Genetic engineering techniques are also available for varying amino acid patterns of a subunit or introducing functional peptide sequences. We have previously demonstrated the introduction of cancer cell targeting moieties or therapeutic agents to several different protein cages (16,31,33,34). It has been reported that "activated" macrophages in an unstable plaque express specific receptors such as a chemokine-receptor, CCR2 (35). If a specific targeting moiety for "activated" macrophages is introduced to the mineralized rHFn, the resultant material might be expected to localize in macrophages within unstable atherosclerotic plaques and serve as a superior diagnostic test to evaluate the inflammatory state or vulnerability of the plaque to rupture. Furthermore, if a therapeutic agent can be co-loaded into the protein cage, the composite material could simultaneously achieve therapeutic effects on atherosclerotic plaques as well as imaging capability.

As described above, the mineralized rHFn is believed to have great potential as a MRI contrast agent. However, it is important to investigate biocompatibility of the material before proceeding to clinical studies. Although the results of the cell viability assay do not show any statistically significant toxicity of the mineralized rHFn compared with Ferumoxides and Ferumoxtran-10, it does show some decrease in cell count. More extensive in vitro and in vivo toxicity investigations are needed in the future and, even though we have used human recombinant protein, it is also critical to address the immunogenicity of the mineralized ferritin. These investigations are currently under way.

CONCLUSION

In conclusion, iron in the form of a synthetically mineralized magnetite (or maghemite) nanoparticle, encapsulated within the protein cage architecture of a recombinant human H chain ferritin (rHFn) shows great promise as an MRI contrast agent. The biotemplating by the ferritin cage results in mineral cores with narrow size distribution and very homogeneous properties. The macrophage uptake in vitro and T_2* MRI properties of the mineralized rHFn compare favorably with known iron oxide MRI contrast agents. This composite material is expected to have great potential as a MRI contrast agent to assess the state of macrophage-rich atherosclerotic plaques in vivo. Future work will be directed toward incorporating cell specific targeting moieties to the rHFn for cell-specific in vivo applications.

ACKNOWLEDGMENT

The authors thank AMAG Pharmaceuticals, Inc., for providing Ferumoxtran-10 (Combidex®).

REFERENCES

1. Li AC, Glass CK. The macrophage foam cell as a target for therapeutic intervention. Nat Med 2002;8:1235–1242.
2. Russell DG. Mycobacterium tuberculosis: here today, and here tomorrow. Nat Rev Mol Cell Biol 2001;2:569–577.
3. Swanson MS, Hammer BK. Legionella pneumophila pathogenesis: a fateful journey from amoebae to macrophages. Annu Rev Microbiol 2000;54:567–613.
4. Sewell KL, Trentham DE. Pathogenesis of rheumatoid-arthritis. Lancet 1993;341:283–286.
5. Harris ED. Mechanisms of disease - rheumatoid-arthritis - pathophysiology and implications for therapy. N Engl J Med 1990;322:1277–1289.
6. Anthony PP, Ishak KG, Nayak NC, Poulsen HE, Scheuer PJ, Sobin LH. Morphology of cirrhosis - definition, nomenclature, and classification. Bull World Health Organ 1977;55:521–540.
7. Ross R. Mechanisms of disease - atherosclerosis - an inflammatory disease. N Engl J Med 1999;340:115–126.
8. Kooi ME, Cappendijk VC, Cleutjens K, Kessels AGH, Kitslaar P, Borgers M, Frederik PM, Daemen M, van Engelshoven JM. Accumulation of ultrasmall superparamagnetic particles of iron oxide in human atherosclerotic plaques can be detected by in vivo magnetic resonance imaging. Circulation 2003;107:2453–2458.
9. Raynal I, Prigent P, Peyramaure S, Najid A, Rebuzzi C, Corot C. Macrophage endocytosis of superparamagnetic iron oxide nanoparticles - mechanisms and comparison of ferumoxides and ferumoxtran-10. Invest Radiol 2004;39:56–63.
10. Yancy AD, Olzinski AR, Hu TC, Lenhard SC, Aravindhan K, Gruver SM, Jacobs PM, Willette RN, Jucker BM. Differential uptake of ferumoxtran-10 and ferumoxytol, ultrasmall superparamagnetic iron oxide contrast agents in rabbit: critical determinants of atherosclerotic plaque labeling. J Magn Reson Imaging 2005;21:432–442.
11. Ruehm SG, Corot C, Vogt P, Kolb S, Debatin JF. Magnetic resonance imaging of atherosclerotic plaque with ultrasmall superparamagnetic particles of iron oxide in hyperlipidemic rabbits. Circulation 2001;103:415–422.
12. Schmitz SA, Taupitz M, Wagner S, Wolf KJ, Beyersdorff D, Hamm B. Magnetic resonance imaging of atherosclerotic plaques using superparamagnetic iron oxide particles. J Magn Reson Imaging 2001;14:355–361.
13. Schmitz SA, Coupland SE, Gust R, Winterhalter S, Wagner S, Kresse M, Semmler W, Wolf KJ. Superparamagnetic iron oxide-enhanced MRI of atherosclerotic plaques in Watanabe hereditable hyperlipidemic rabbits. Invest Radiol 2000;35:460–471.
14. Douglas T, Strable E, Willits D, Aitouchen A, Libera M, Young M. Protein engineering of a viral cage for constrained nanomaterials synthesis. Adv Mater 2002;14:415–418.
15. Gilmore K, Idzerda YU, Klem MT, Allen M, Douglas T, Young M. Surface contribution to the anisotropy energy of spherical magnetite particles. J Appl Phys 2005;97.
16. Uchida M, Flenniken ML, Allen M, Willits DA, Crowley BE, Brumfield S, Willis AF, Jackiw L, Jutila M, Young MJ, Douglas T. Targeting of cancer cells with ferrimagnetic ferritin cage nanoparticles. J Am Chem Soc 2006;128:16626–16633.
17. Klem MT, Willits D, Solis DJ, Belcher AM, Young M, Douglas T. Bio-inspired synthesis of protein-encapsulated CoPt nanoparticles. Adv Funct Mate 2005;15:1489–1494.
18. Douglas T, Young M. Viruses: making friends with old foes. Science 2006;312:873–875.
19. Allen M, Bulte JW, Liepold L, Basu G, Zywicke HA, Frank JA, Young M, Douglas T. Paramagnetic viral nanoparticles as potential high-relaxivity magnetic resonance contrast agents. Magn Reson Med 2005;54:807–812.
20. Liepold L, Anderson S, Willits D, Oltrogge L, Frank JA, Douglas T, Young M. Viral capsids as MRI contrast agents. Magn Reson Med 2007;58:871–879.
21. Hooker JM, Datta A, Botta M, Raymond KN, Francis MB. Magnetic resonance contrast agents from viral capsid shells: a comparison of exterior and interior cargo strategies. Nano Lett 2007;7:2207–2210.
22. Prasuhn DE Jr, Yeh RM, Obenaus A, Manchester M, Finn MG. Viral MRI contrast agents: coordination of Gd by native virions and attachment of Gd complexes by azide-alkyne cycloaddition. Chem Commun (Camb) 2007:1269–1271.
23. Anderson EA, Isaacman S, Peabody DS, Wang EY, Canary JW, Kirshenbaum K. Viral nanoparticles donning a paramagnetic coat: conjugation of MRI contrast agents to the MS2 capsid. Nano Lett 2006;6:1160–1164.
24. Mitchell MD, Kundel HL, Axel L, Joseph PM. Agarose as a tissue equivalent phantom material for NMR imaging. Magn Reson Imaging 1986;4:263–266.

25. Harrison PM, Arosio P. Ferritins: molecular properties, iron storage function and cellular regulation. Biochim Biophys Acta-Bioenergetics 1996;1275:161–203.
26. Bulte JW, Douglas T, Mann S, Frankel RB, Moskowitz BM, Brooks RA, Baumgarner CD, Vymazal J, Strub MP, Frank JA. Magnetoferritin - characterization of a novel superparamagnetic MR contrast agent. J Magn Reson Imaging 1994;4:497–505.
27. Lawson DM, Artymiuk PJ, Yewdall SJ, Smith JM, Livingstone JC, Treffry A, Luzzago A, Levi S, Arosio P, Cesareni G, Thomas CD, Shaw WV, Harrison PM. Solving the structure of human H-ferritin by genetically engineering intermolecular crystal contacts. Nature 1991;349:541–544.
28. Lim JH, Choi D, Cho SK, Kim SH, Lee WJ, Lim HK, Park CK, Paik SW, Kim YI. Conspicuity of hepatocellular nodular lesions in cirrhotic livers at ferumoxides-enhanced MR imaging: importance of Kupffer cell number. Radiology 2001;220:669–676.
29. Ros PR, Freeny PC, Harms SE, Seltzer SE, Davis PL, Chan TW, Stillman AE, Muroff LR, Runge VM, Nissenbaum MA, Jacobs PM. Hepatic MR-imaging with ferumoxides - a multicenter clinical-trial of the safety and efficacy in the detection of focal hepatic-lesions. Radiology 1995;196: 481–488.
30. Jung CW, Jacobs P. Physical and chemical-properties of superparamagnetic iron-oxide MR contrast agents - ferumoxides, ferumoxtran, ferumoxsil. Magn Reson Imaging 1995;13:661–674.
31. Flenniken ML, Willits DA, Harmsen AL, Liepold LO, Harmsen AG, Young MJ, Douglas T. Melanoma and lymphocyte cell-specific targeting incorporated into a heat shock protein cage architecture. Chem Biol 2006;13:161–170.
32. Chatterji A, Burns LL, Taylor SS, Lomonossoff GP, Johnson JE, Lin T, Porta C. Cowpea mosaic virus: from the presentation of antigenic peptides to the display of active biomaterials. Intervirology 2002;45:362–370.
33. Flenniken ML, Willits DA, Brumfield S, Young M, Douglas T. The small heat shock protein cage from methanococcus jannaschii is a versatile nanoscale platform for genetic and chemical modification. Nano lett 2003;3:1573–1576.
34. Flenniken ML, Liepold LO, Crowley BE, Willits DA, Young MJ, Douglas T. Selective attachment and release of a chemotherapeutic agent from the interior of a protein cage architecture. Chem Commun 2005:447–449.
35. Gerard C, Rollins BJ. Chemokines and disease. Nat Immunol 2001;2: 108–115.